Supplementary Information

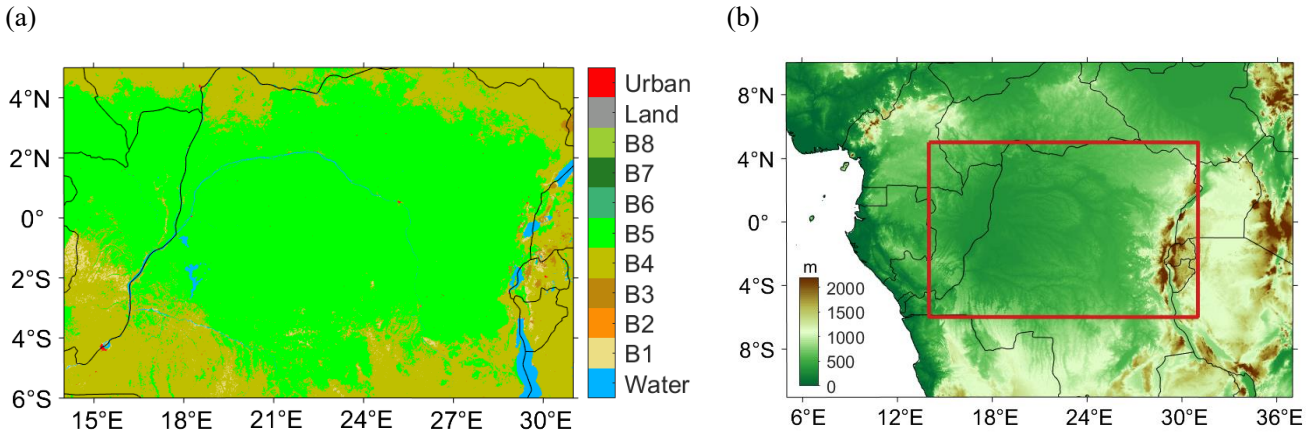

Figure S1. (a) Landcover of the Congo Basin (5°N-6°S, 14°E-31°E) in Year 2010 according to the MODIS LAI classification scheme. It stratifies the global vegetation into eight architectural types, or biomes: grasslands (B1), shrublands (B2), broadleaf croplands (B3), savannas (B4), evergreen broadleaf forest (B5), deciduous broadleaf forests (B6), evergreen needleleaf forests (B7), deciduous needleleaf forests (B8). Biome types present in the Congo Basin are evergreen broadleaf forest (B5) and savannas (B4). (b) Terrain elevation from SRTM dataset. Our study area is shown as a red rectangle. Elevation of a highland region in the southeast part of the study area varies between 530 m and 1728 m. This area represents a montane ecosystem.

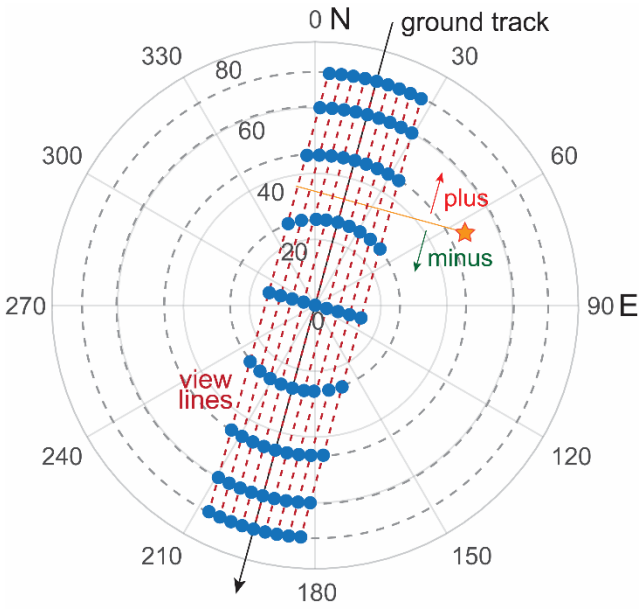

Figure S2. Sun-sensor geometry of MISR observations on the polar plane. Direction from a point on the Earth surface to Sun is shown as a star. The MISR instrument uses nine separate forward-, nadir- and aft-looking push broom cameras to acquire data at nine along-track view zenith angles of 0.0^o (camera An), 26.1^o (Af and Aa), 45.6^o (Bf and Ba), 60.0^o (Cf and Ca) and 70.5^o (Df and Da). Each camera sees instantaneously a single row of pixels at right angles to the ground track, resulting in a 360 km cross-track swath. MISR along-track observation angles form lines on the polar plane, which are characterized by a slope, *k*, and intercept, *b*. The slope is constant (k~tan(15.4^o)) and coincides with the ground track direction (~15.4^o). The intercept is associated with location of pixel within the 360 km swath that cameras see. We express BRF as a function of the phase angle, which is the angle between directions to the sun and sensor. We assign the sign "plus" to the phase angle if the direction to the MISR sensor approaches the direction to sun from North, and "minus" otherwise. In this sun-tracking coordinates the MISR Bidirectional Reflectance Factor (BRF) is a function of SZA, phase angle and MISR view line, the latter is specified by VZA of the MISR nadir camera.

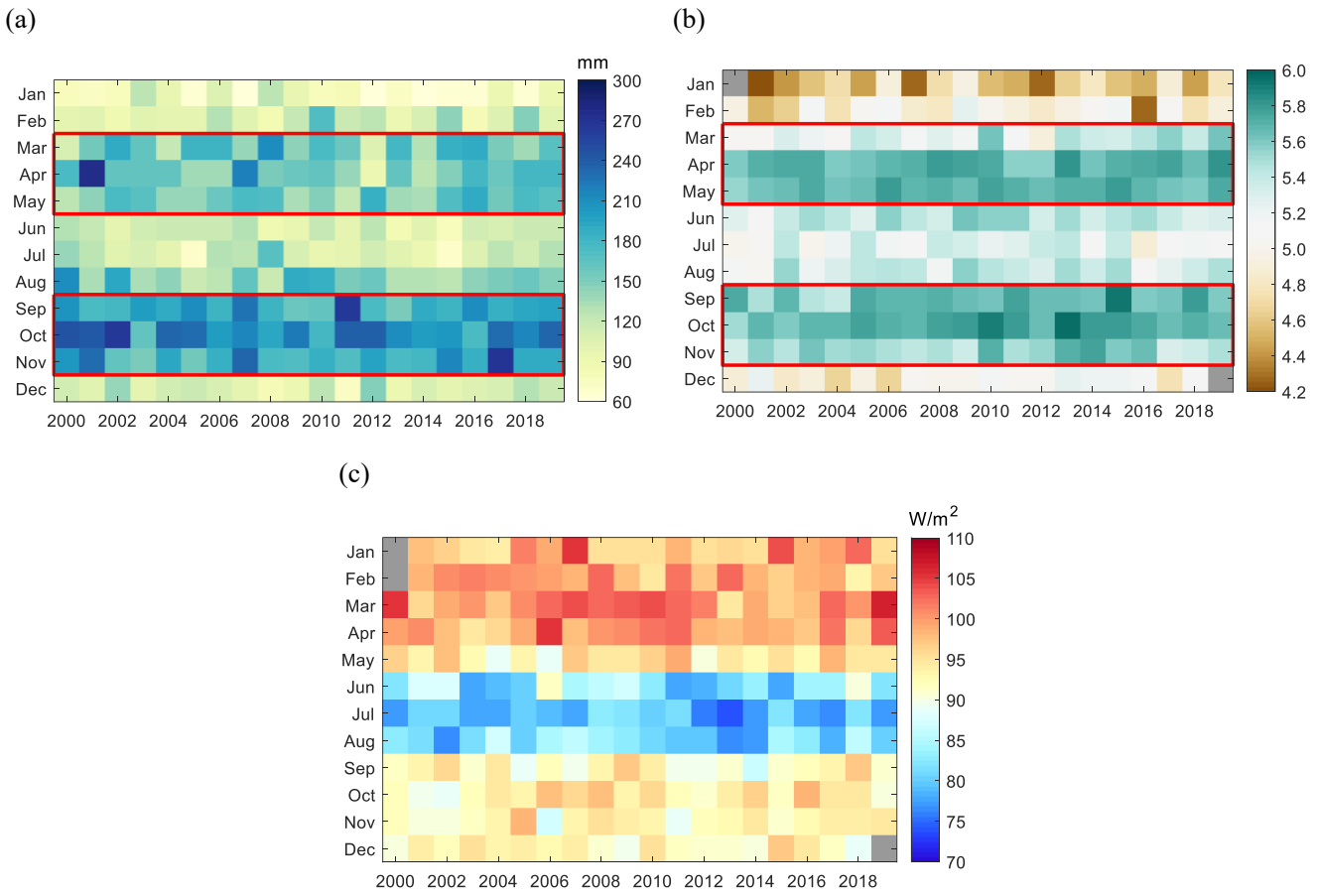

Figure S3. Seasonality of (a) monthly precipitation from TRMM, (b) LAI from MODIS C6 and (c) PAR from CERES over the Congolese forests in the past two decades (2000-2019). Months with no data are labeled with grey color in the color maps. A bimodal seasonal cycle is clearly seen in the rainfall and the LAI color maps. The first peak in precipitation and LAI occurred in March-April-May (wet season 1) and the second in September-October-November (wet season 2). Wet season periods are marked with red square in the (a) and (b).

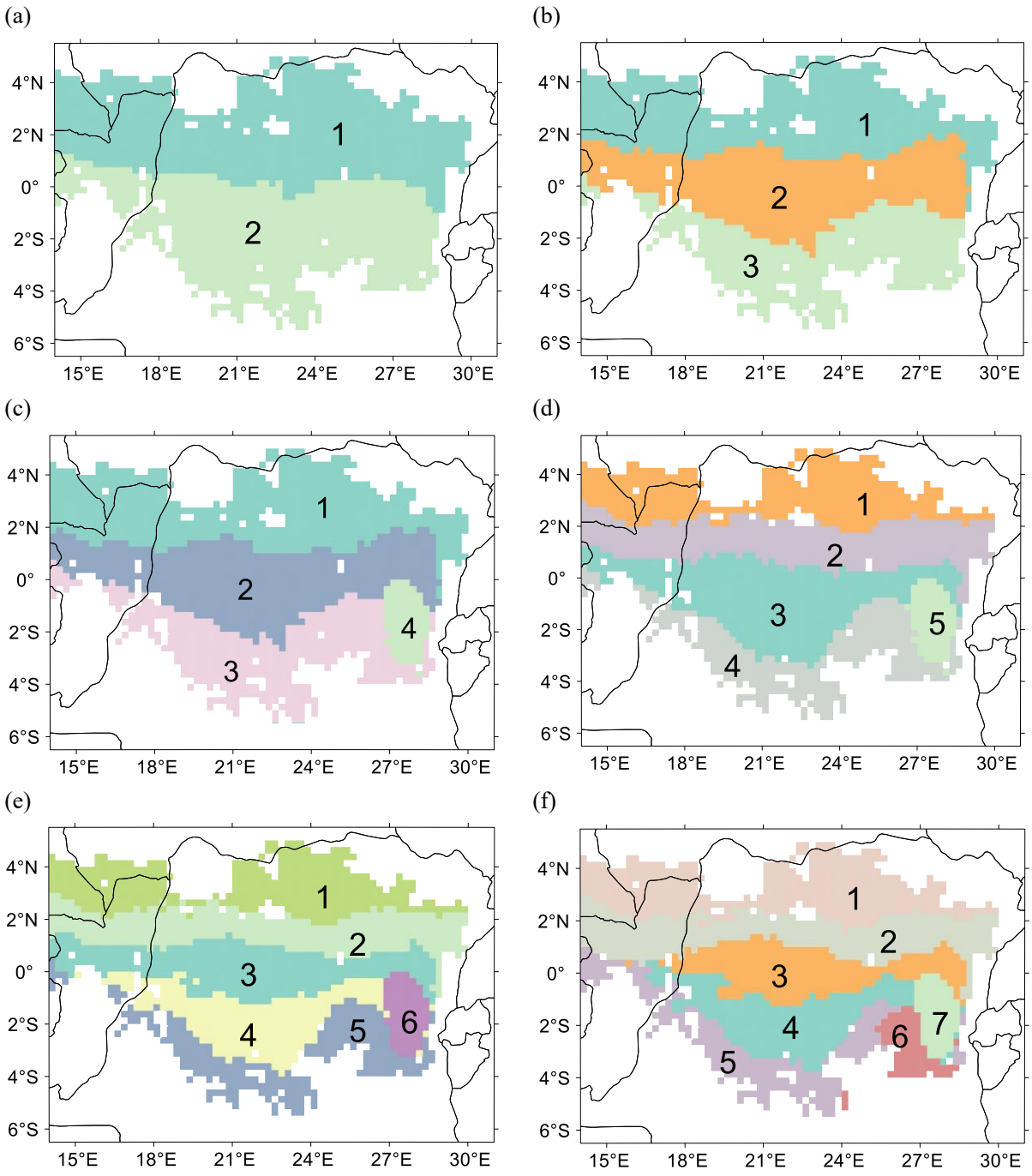

Figure S4. Partitioning of the study area into 2 to 7 clusters. K-Means clustering method with mean monthly climatology data of precipitation, PAR and LAI as input was used. Boundaries of clusters are generally parallel to the Equator. A highland region in the southeast part the Congolese forest (Figure S1) appeared in partitioning our study area into 4 and more clusters. An increase in the number of clusters lowers cluster areas, which in turn may not contain enough satellite observations for statistical analyses. We use the four-cluster partition in our analyses.

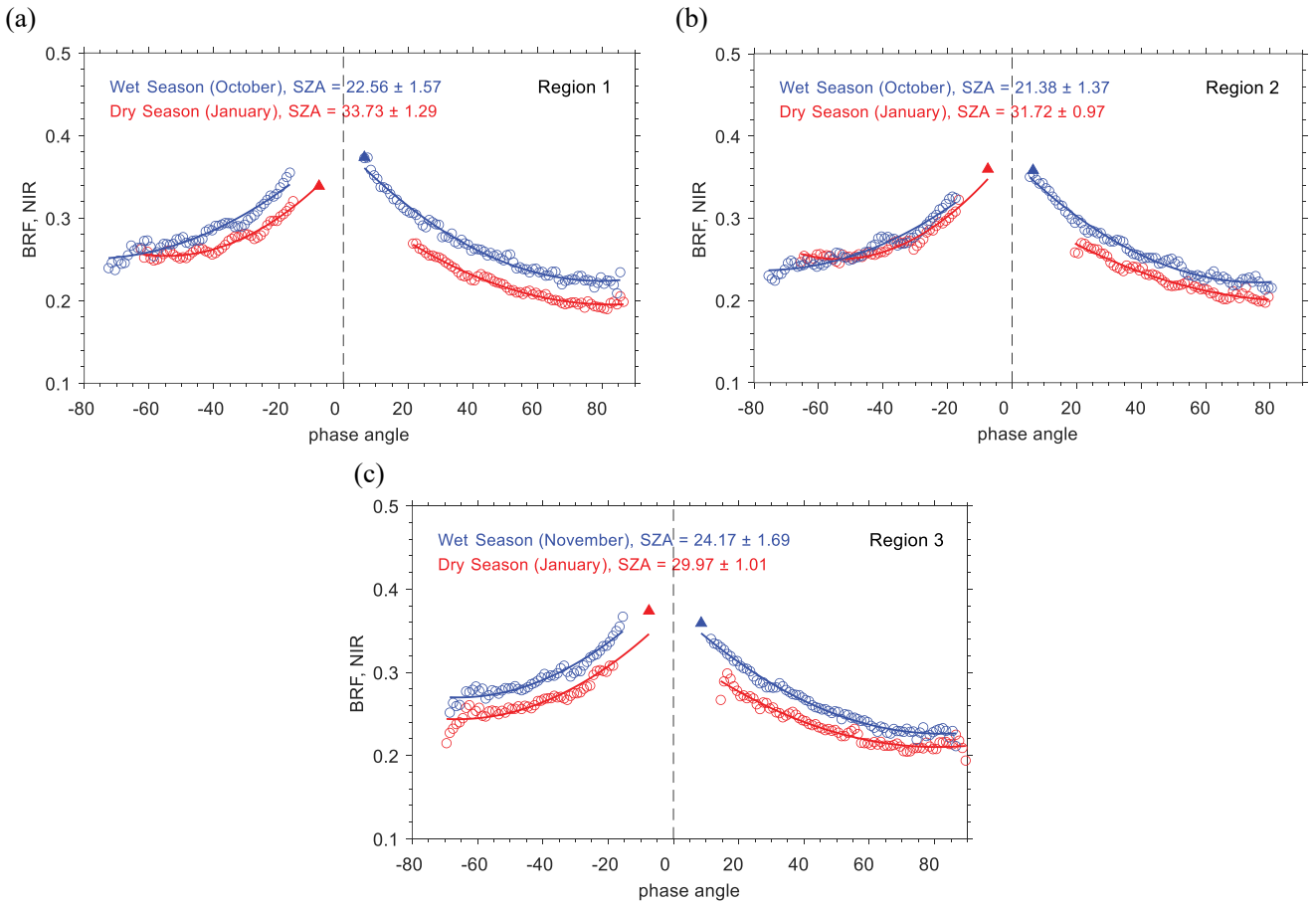

Figure S5. MISR BRF and DSCOVR BRF at NIR spectral bands during the wet and dry seasons over region 1 (panel a), region 2 (panel c) and region 3 (panel c). Note that a higher or equal reflectance at lower SZA relative to reflectance at higher SZA always indicates an increase in leaf area and foliage scattering properties according to the physics of radiation interaction in vegetation (Bi et al., 2015). Such a behavior is clearly seen in BRF of region 2.

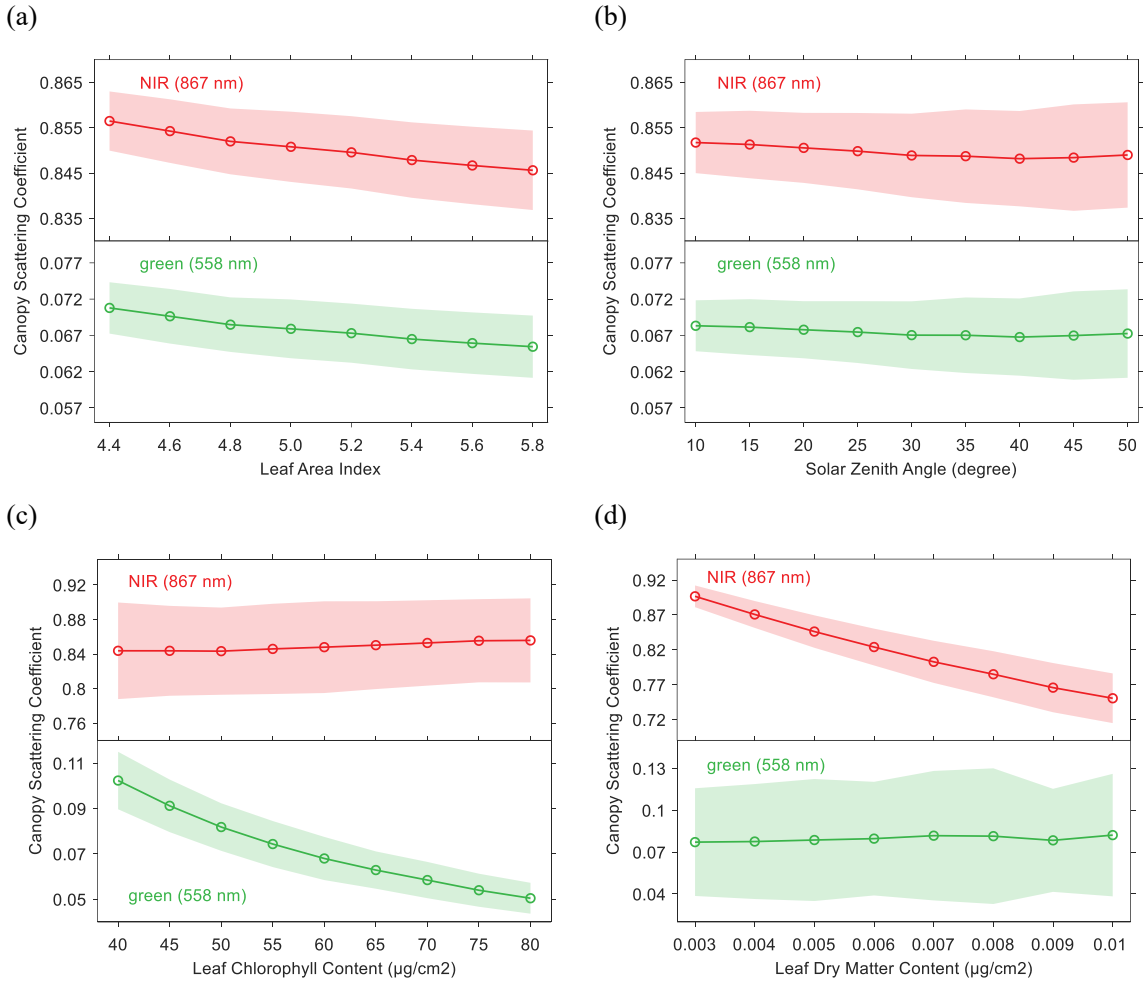

Figure S6. Sensitivity of the canopy scattering coefficient to (a) LAI, LAI>4.4, (b) SZA, (c) leaf chlorophyll content and (d) leaf dry matter content in green (558nm) and NIR (867 nm) derived based on the PROSAIL model (Jacquemoud et al. 2009). The shaded area represents the ±1 standard deviation error. The canopy scattering coefficient is almost insensitive to LAI and SZA, but exhibits strong sensitive to leaf chlorophyll and dry matter contents in green (558 nm) and NIR (867 nm), respectively.

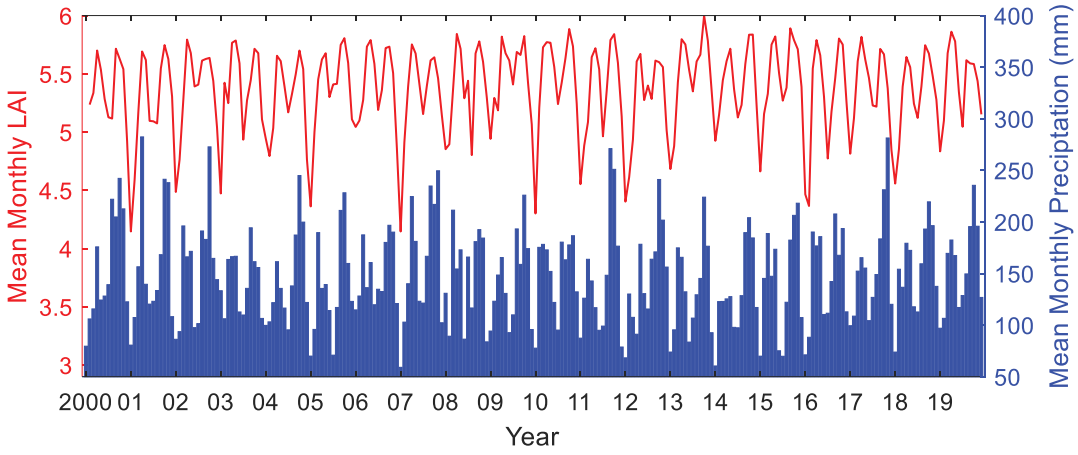

Figure S7. Time series of monthly LAI and precipitation from 2000 to 2019 over the Congolese forests. The MODIS Collection 6 LAI product and TRMM 3B43 version 7 data were used to generate monthly average LAI and precipitation time series as described in Section 2. The monthly LAI and precipitation are strongly positively correlated ($R=0.67$, $P<0.01$), suggesting a direct and instant impact of water availability on the functionality the Congolese forests.

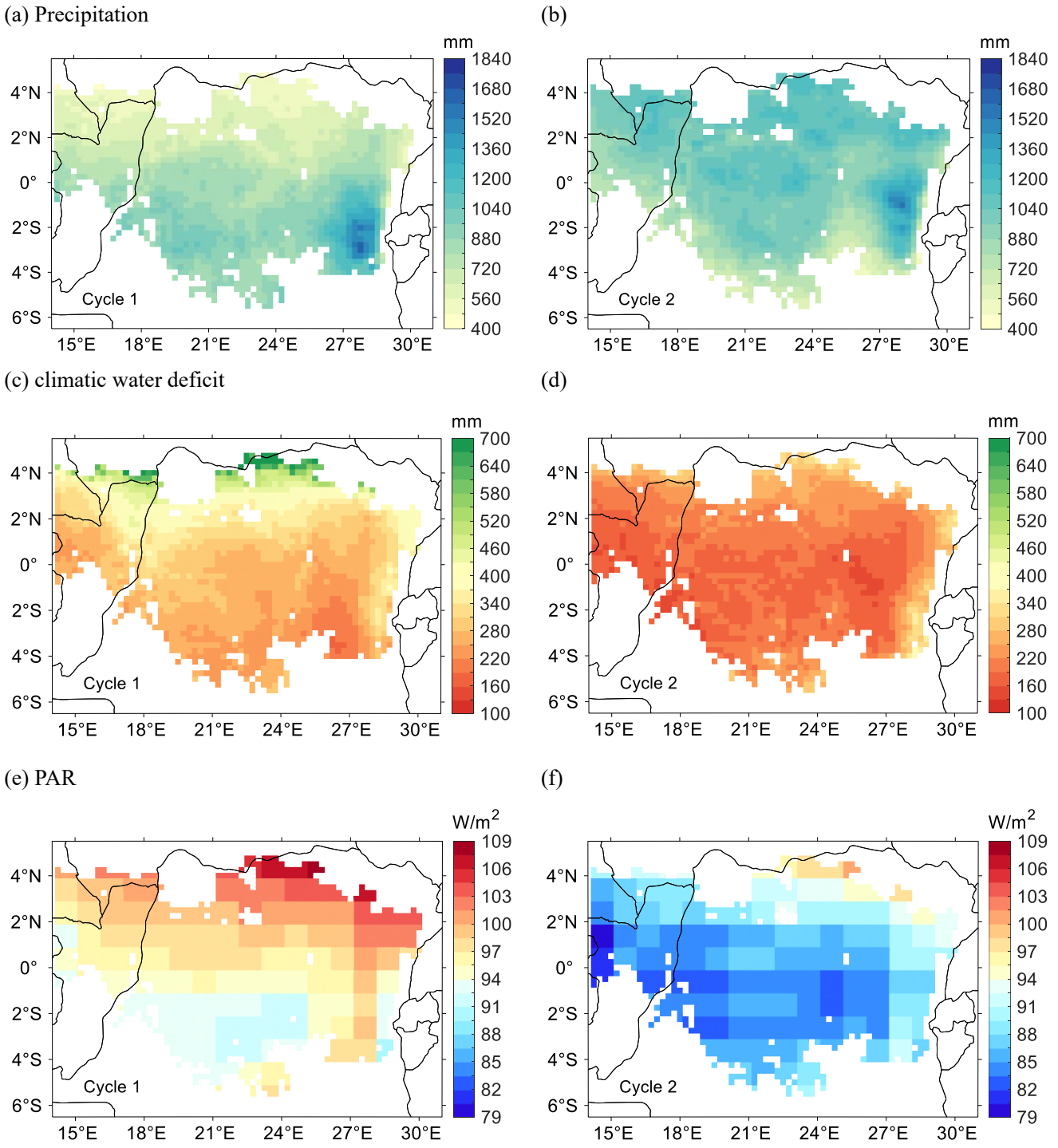

Figure S8. Distribution of precipitation, climatic water deficit and PAR during seasonal cycles 1 (December to June, left panels) and 2 (June to December, right panels).

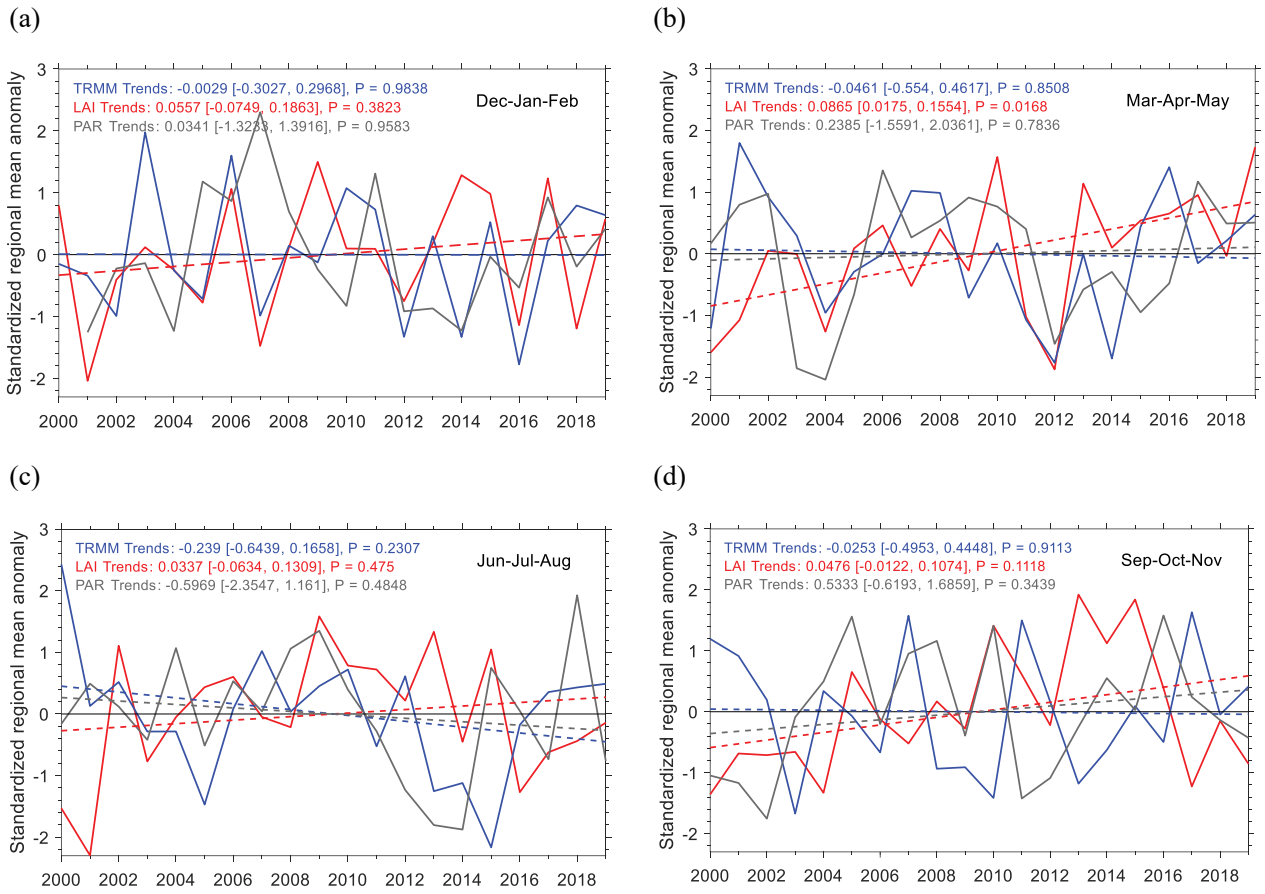

Figure S9. Standardized regional mean anomalies in seasonal precipitation, LAI and PAR for seasonal cycles 1 (upper panels) and 2 (lower panels) over the entire Congolese forests for the period of 2000-2019. Values of linear trends (with 95% confidence interval) per decade and their significant levels, P, are shown in legends. There are no significant declines or increases in precipitation and PAR for the past two decades. All seasons have shown an increase in LAI with a higher P-values during wet seasons.

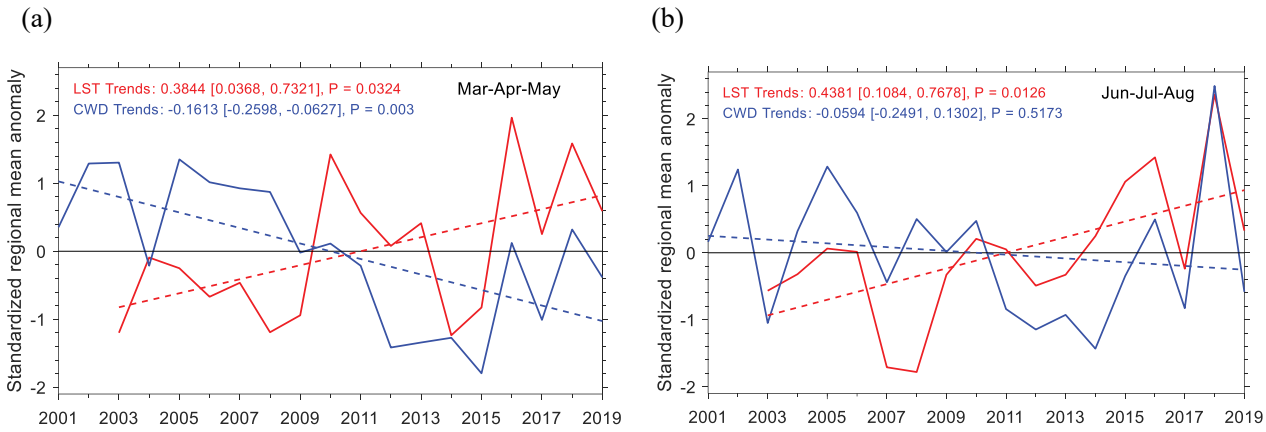

Figure S10. Standardized regional mean anomalies in seasonal land surface temperature (LST) and climatic water deficit (CWD) over the focus region (0.5°N-2.5°S, 25.5°E-28.5°E) for the past two decades in wet season 1 (MAM) and dry season 2 (JJA). The linear trend (with 95% confidence interval) per decade and its significant level P are shown.